Using Hierarchic Interpolation With Mortar Element Method for Electrical Machines Analysis

Orlando Jose Antunes[1], J. P. A. Bastos[2], N. Sadowski[2], A. Razek[3], L. Santandrea[3], F. Bouillault[3], and F. Rapetti[4]

[1]Centro Federal de Educação Tecnologica de Santa Catarina, Florianopolis, SC, Brazil
[2]Universidade Federal de Santa Catarina, GRUCAD/EEL/CTC, 88040-900 Florianopolis, SC, Brazil
[3]LGEP-UMR 8507 CNRS, Paris VI, Paris XI Univ. and Supelec, Plateau de Moulon, 91192 Gif-sur-Yvette cedex, France
[4]Lab. De Mathématiques-UMR 6621 CNRS, Nice-Sophia Antipolis Univ., Parc Valrose, 06108 Nice cedex 2, France

This work analyzes the use of the mortar element method and moving band technique to perform the movement in electrical machines. To improve the accuracy of the methods, high order hierarchic interpolation is used on the interface between moving and fixed parts. Results with first, second, and third order hierarchic interpolation are shown in order to compare conforming and nonconforming approaches.

***Index Terms*—Hierarchic elements, mortar element method, moving band method.**

I. Introduction

THERE are several methods to take into account the movement in electrical machines, but if no constraints are imposed between the time step and the element size at the slip surface (which is commonly necessary to coupled problems), only a few of them can be used successfully. Among them the moving band technique (MB) [1], when used with high order lagrange or hierarchic elements, produces excellent e.m.f. results even with strong distortion of the elements in thin airgap machines. Continuing our investigations, we analyze here the performance of the mortar element method (MEM), used recently for electromagnetic analysis [2] and we compare it with the MB using high order interpolation. A main contribution of this paper is the inclusion of hierarchic interpolation as well as the application of (anti)periodicity conditions using the classical MEM formulation, which is originally applied only for a closed slip surface. The MEM, as the MB, does not increase the size of the resultant system, and produces a positive definite and sparse matrix, allowing the free movement of the rotor without constraints in the time step.

II. Mortar Element Method

The MEM considers two independent meshes that are connected by a sliding interface Γ. These meshes are condensed independently as in the traditional finite element method. One mesh is considered the slave and the other the master. We choose rotor as the master and stator as the slave (Fig. 1). The vector potential on the slave interface side $\mathbf{A}_s^\Gamma$ is function of master interface side $\mathbf{A}_m^\Gamma$. The basis of the MEM is found in [3] and it may be expressed by

$$\mathbf{A}_s^\Gamma = \mathbf{Q}\mathbf{A}_m^\Gamma \tag{1}$$

where

$$\mathbf{Q} = \mathbf{C}^{-1}\mathbf{D}. \tag{2}$$

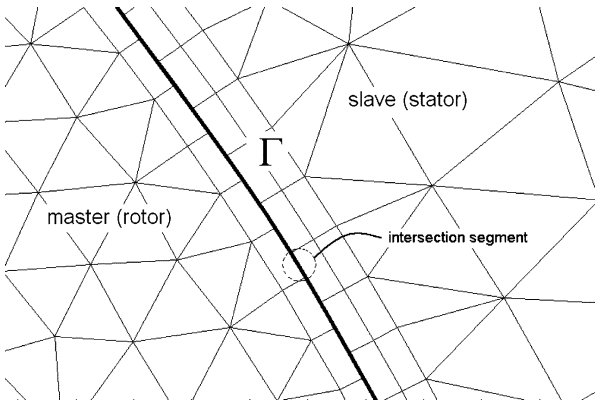

Fig. 1. Discretization scheme of MEM.

$\mathbf{C}$ and $\mathbf{D}$ may be calculated by line integrals over Γ

$$\mathbf{C}(i,j) = \int_\Gamma \psi_i \psi_j d\Gamma \quad \mathbf{D}(i,j) = \int_\Gamma \varphi_j \psi_i d\Gamma. \tag{3}$$

The functions ψ_i and φ_i are the base functions of slave and master, respectively, whose support is on the union of mortar elements. The mortar elements appear between the slave and the master meshes having, at least, one node on Γ. As the potentials at the nodes of the slave interface $\mathbf{A}_s^\Gamma$ are functions of the potentials on the master interface, they can be eliminated in the final system. The potentials over the whole domain, slave and master, can be linked as follows:

$$\begin{bmatrix} \mathbf{A}_s^\Gamma \\ \mathbf{A}_s \\ \mathbf{A}_m^\Gamma \\ \mathbf{A}_m \end{bmatrix} = \begin{bmatrix} \mathbf{0} & \mathbf{Q} & \mathbf{0} \\ \mathbf{Id} & \mathbf{0} & \mathbf{0} \\ \mathbf{0} & \mathbf{Id} & \mathbf{0} \\ \mathbf{0} & \mathbf{0} & \mathbf{Id} \end{bmatrix} \begin{bmatrix} \mathbf{A}_s \\ \mathbf{A}_m^\Gamma \\ \mathbf{A}_m \end{bmatrix} \tag{4}$$

which can be noted as

$$\mathbf{A} = \widetilde{\mathbf{Q}}\overline{\mathbf{A}} \tag{5}$$

where $\widetilde{\mathbf{Q}}$ is the coupling matrix, $\mathbf{Id}$ is the identity matrix, and $\mathbf{A}_s$ and $\mathbf{A}_m$ are the potentials out of the interface in the slave and master meshes, respectively.

Digital Object Identifier 10.1109/TMAG.2005.844561

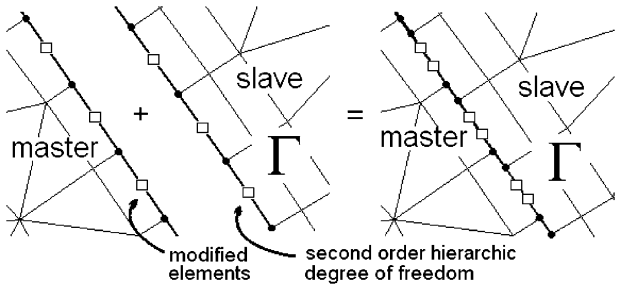

Fig. 2. Linking slave and master meshes with second order hierarchic interpolation on Γ.

Applying the coupling matrix on the original finite element system $\mathbf{MA} = \mathbf{S}$, we have

$$\widetilde{\mathbf{Q}}^T\mathbf{M}\widetilde{\mathbf{Q}}\overline{A} = \widetilde{\mathbf{Q}}^T\mathbf{S}. \tag{6}$$

The resultant system above is sparse and positive definite. So, it can be easily solved by iterative methods.

Considering the radius ρ of Γ very long, when compared with one edge on the interface, a matrix $\mathbf{C}$ may be constructed for first order interpolation by assembling the following local matrix:

$$c_{\text{local}} = \int_{\theta s_1}^{\theta s_2} \begin{bmatrix} \psi_1\psi_1 & \psi_1\psi_2 \\ \psi_2\psi_1 & \psi_2\psi_2 \end{bmatrix} \rho d\theta \tag{7}$$

$$\psi_1 = \frac{\theta s_2 - \theta}{\theta s_2 - \theta s_1} \quad \text{and} \quad \psi_2 = s\frac{\theta - \theta s_1}{\theta s_2 - \theta s_1} \tag{8}$$

where θ_{s1} and θ_{s2} are the node angles of one element edge on the slave interface side. For (anti)periodicity $s = -1$ on the last slave edge of Γ and $s = 1$ elsewhere. For matrix $\mathbf{D}$, we have

$$d_{\text{local}} = \int_{\theta_1}^{\theta_2} \begin{bmatrix} \psi_1\varphi_1 & \psi_1\varphi_2 \\ \psi_2\varphi_1 & \psi_2\varphi_2 \end{bmatrix} \rho d\theta \tag{9}$$

$$\varphi_1 = n\frac{\theta m_2 - \theta}{\theta m_2 - \theta m_1} \quad \text{and} \quad \varphi_2 = n\cdot m\frac{\theta - \theta m_1}{\theta m_2 - \theta m_1} \tag{10}$$

where θ_1 and θ_2 are the node angles of a intersection segment between slave and master edges (see Fig. 1) and θ_{m1} and θ_{m2} are the node angles of one element edge on the master interface side. For (anti)periodicity $m = -1$ on the last master edge of Γ and $m = +1$ elsewhere. To find the intersection segments when computing the integral (9), it is necessary to perform two searches: the first is with the rotor [one pole for (anti)periodicity condition] at the actual position $(n = +1)$ and the second with the rotor displaced of total domain angle $(n = -1)$.

III. Mortar Element Method With Hierarchic Interpolation

The use of high order interpolation on Γ increases the accuracy of the normal component of the magnetic induction and thus ensures its conservation more efficiently.

We use hierarchic functions due to the orthogonality of the Legendre polynomials, which produce a better conditioned system than lagrange elements. To use high order interpolation only on the interface Γ, modified elements appears close to it (Fig. 2). Hierarchic interpolation is also convenient to generate the interpolation functions for this type of element: it is only necessary to add one degree of freedom on the edge on the interface without changes in the original first order functions. The local contributions for matrices $\mathbf{C}$ and $\mathbf{D}$ with second order hierarchic interpolation on Γ are

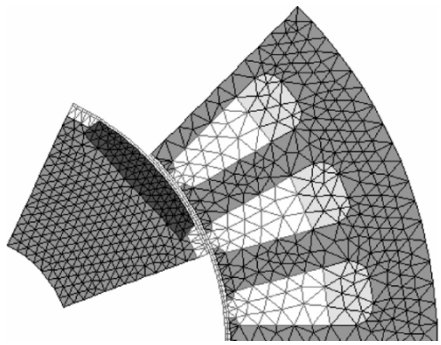

Fig. 3. Brushless DC motor mesh.

$$c_{\text{local}} = \int_{\theta s_1}^{\theta s_2} \begin{bmatrix} \psi_1\psi_1 & \psi_1\psi_2 & \psi_1\psi_3 \\ \psi_2\psi_1 & \psi_2\psi_2 & \psi_2\psi_3 \\ \psi_3\psi_1 & \psi_3\psi_2 & \psi_3\psi_3 \end{bmatrix} \rho d\theta \tag{11}$$

with $\psi_3 = |\psi_1\psi_2|$ and

$$d_{\text{local}} = \int_{\theta_1}^{\theta_2} \begin{bmatrix} \psi_1\varphi_1 & \psi_1\varphi_2 & \psi_1\varphi_3 \\ \psi_2\varphi_1 & \psi_2\varphi_2 & \psi_2\varphi_3 \\ \psi_3\varphi_1 & \psi_3\varphi_2 & \psi_3\varphi_3 \end{bmatrix} \rho d\theta \tag{12}$$

where $\varphi_3 = n|\varphi_1\varphi_2|$.

For cubic interpolation on Γ, the hierarchic functions are $\psi_4 = |\psi_1\psi_2|(|\psi_2| - \psi_1)$ and $\varphi_4 = n|\varphi_1\varphi_2|(|\varphi_2| - |\varphi_1|)$.

IV. Results

A. Brushless DC Motor

For this machine, the mesh shown in Fig. 3 is used. This motor has an airgap of 0.7 mm in which the upper side is iron and the lower side the magnet.

To compare the methods, the same mesh is used for both cases, with 39 edges on both sides of the interface. The rotor displacement step is set in a way that five steps are necessary to overpass one element on Γ. Fig. 4 shows better results with the MEM than MB, for first order interpolation on Γ.

As shown in Fig. 4, the experimental and simulation results are in very good agreement. Only with a zoom can we see the oscillations due to the movement. With second order the oscillations due to the movement are eliminated in the two methods.

B. Thin Airgap Synchronous Machine

For this machine, which has a thin airgap (0.3 mm) with iron in both sides, two discretizations are used: mesh 1 with 81 edges (Fig. 5) and mesh 2 with 162 edges on both interface sides. The airgap has two layers of quadrilaterals elements. The interface Γ is placed between them for MEM and the MB is placed in the lower one. Although a nonregular mesh in the airgap (dense near the rotor tooth corners and coarse in the airgap regions between tooth) may produce better magnetic induction results concerning torque evaluation, for the e.m.f., as it is calculated on the coils (relatively far from de airgap), a regular mesh avoids very

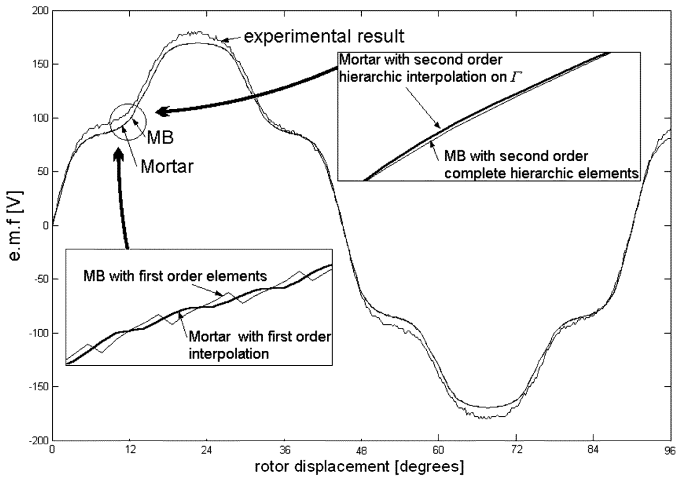

Fig. 4. Electromotive force for a brushess DC motor.

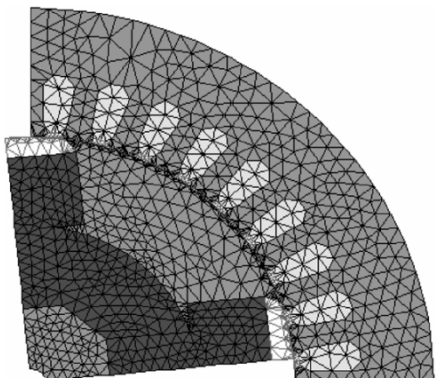

Fig. 5. Thin air gap synchronous machine with polar pieces. Mesh 1 with 81 edges on Γ.

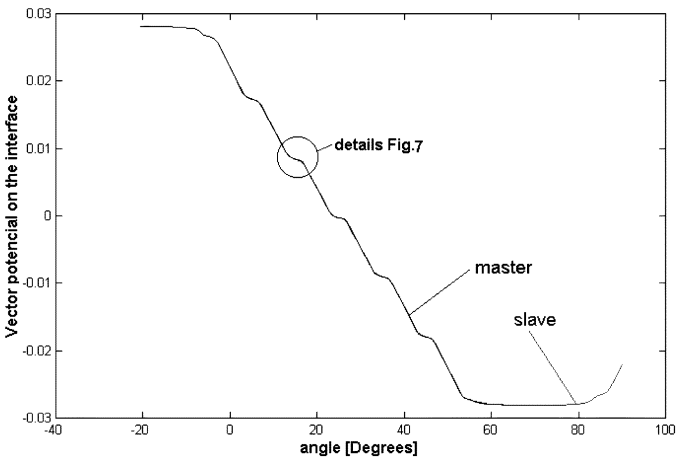

Fig. 6. Continuity of the vector potential on the interface Γ for first order interpolation (mesh 1).

deformed elements (producing discontinuities) and the final results are better with the regular mesh. Initially, we tested the continuity of the potential vector on the interface with the rotor placed at 20.5 degrees. For this angle there is no conformity between slave and master meshes for MEM.

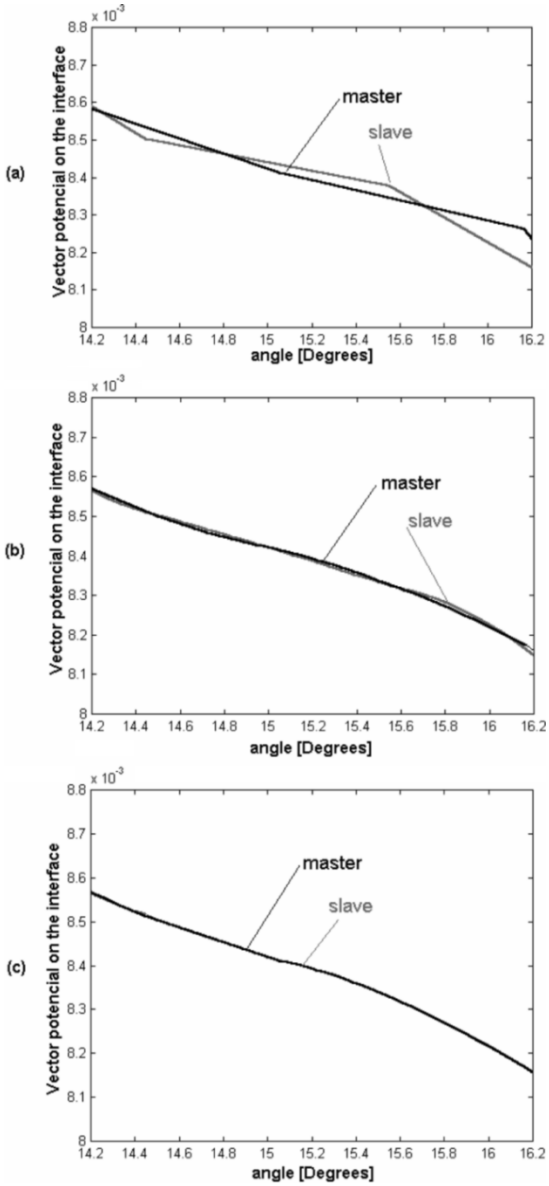

Fig. 7. Details of Fig. 6 for (a) first, (b) second and (c) third order interpolation on Γ.

Fig. 6 shows that slave and master potentials are very close. Only with zoom (Fig. 7) is it possible to see small discontinuities with first order interpolation. For the second as well as the third order, the continuity is more strongly obtained.

The results in Fig. 8 for mesh 1 show again a better result with MEM compared to the MB for first order interpolation. The rotor displacement step is set in a way that 10 steps are necessary to overpass one element on Γ.

For this machine, to obtain a result with a low intensity of numeric noise is necessary a denser mesh. Figs. 9–11 show the e.m.f. results for mesh 2 between 37.2 and 48 degrees, where the noise is intense. It is clear that, like for mesh 1, the difference between MEM and MB is more evident with first order interpolation. However, Table I shows that MB is faster than MEM, in particular with high order interpolation. There is no significant difference between cubic and second order interpolation.

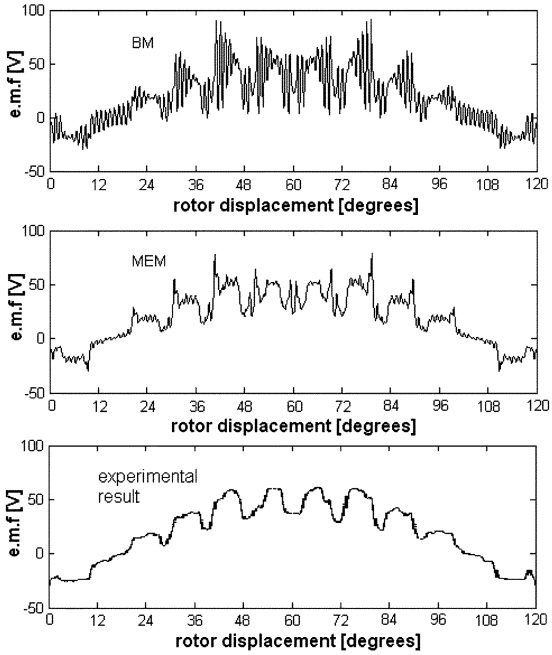

Fig. 8. E.m.f. with mesh 1. MB with first order elements and MEM with first order interpolation on Γ.

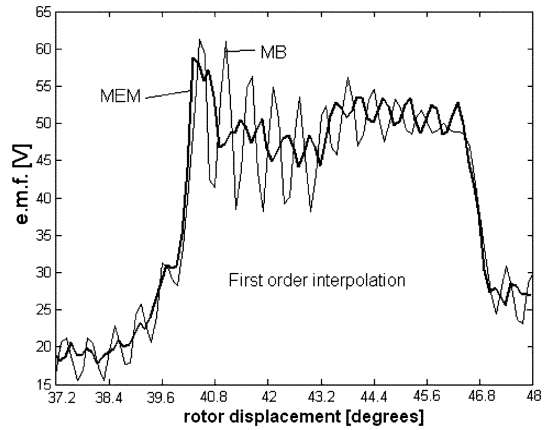

Fig. 9. E.m.f. with mesh 2. MB with first order elements and MEM with first order interpolation on Γ.

So, the cubic interpolation, with its computational cost, is not advantageous in this case.

V. Conclusion

This work shows that it is possible to obtain good e.m.f. results in thin airgap machines by using MEM with high order elements. The MEM produces better results than MB for the same discretization. However, MB is faster than MEM. It is necessary observe that, for the thin airgap synchronous machine, two layers of elements in the airgap were used. This is necessary to avoid the interface on the iron/air boundary, where the errors on the solution may increase, since the continuity of vector potential is assured in an average sense for the MEM. But, this is not a limitation for the MB and, as shown in [1], good results are obtained with one layer of elements in the airgap by using high order elements. However, if we wish to calculate the electromagnetic torque (which is not accurate if calculated inside the MB), two layers are also necessary.

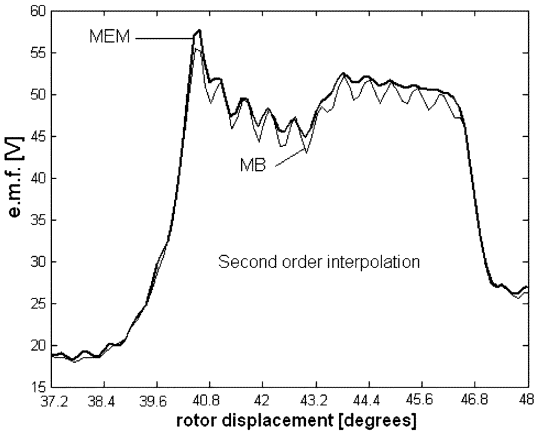

Fig. 10. E.m.f. with mesh 2. MB with second order complete elements and MEM with second order interpolation on Γ.

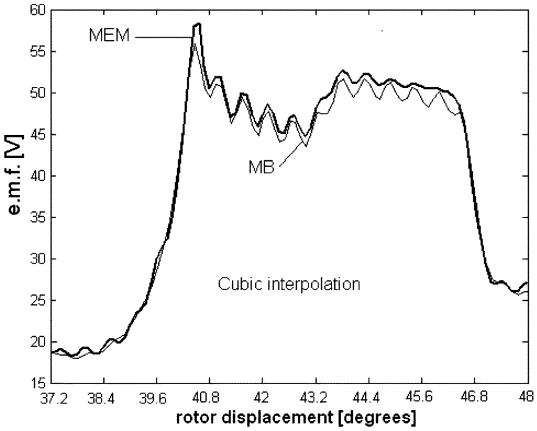

Fig. 11. E.m.f. with mesh 2. MB with cubic complete elements and MEM with cubic interpolation on Γ.

TABLE I
Computation Time

	order	mesh 1	mesh 2
Total number of nodes		1011	1688
Computation Time[s] MEM/ICCG	first	.31	.47
	second	.83	1.62
Computation Time[s] MB/ICCG	first	.09	.15
	second	.15	.25

References

[1] O. J. Antunes, J. P. A. Bastos, and N. Sadowski, "Using high-order finite elements in problems with movement," *IEEE Trans. Magn.*, vol. 40, no. 2, pp. 529–532, Mar. 2004.

[2] M. Taferguenit, L. Santandrea, F. Rapetti, F. Bouillault, and M. Gabsi, "Two methods to take into account the movement within a finite element modelization of an electrical device," in *Proc. Eur. Symp. Num. Meth. in Electromagn. (JEE)*, Toulouse, France, Mar. 2002, pp. 19–24.

[3] F. Rapetti, F. Bouillault, L. Santandrea, A. Buffa, Y. Maday, and A. Razek, "Calculation of eddy currents with edge elements on non-matching grids in moving structures," *IEEE Trans. Magn.*, vol. 36, no. 4, pp. 1351–1355, Jul. 2000.

Manuscript received June 8, 2004.